Development/Plasticity/Repair

# Genetic, Cellular, and Functional Evidence for $Ca^{2+}$ Inflow through $Ca_v1.2$ and $Ca_v1.3$ Channels in Murine Spiral Ganglion Neurons

**Ping Lv,[1,2] Hyo Jeong Kim,[1] Jeong-Han Lee,[1] Choong-Ryoul Sihn,[1] Somayeh Fathabad Gharaie,[1] Atefeh Mousavi-Nik,[1] Wenying Wang,[1] Hong-Gang Wang,[3] Michael Anne Gratton,[4] Karen J. Doyle,[1] Xiao-Dong Zhang,[5] Nipavan Chiamvimonvat,[5,6] and Ebenezer N. Yamoah[1]**

[1]University of California, Davis, School of Medicine, Center for Neuroscience, Program in Communication Science, Davis, California 95618, [2]Department of Pharmacology, Hebei Medical University, Shijiazhuang, China 050017, [3]Department of Medicine, Division of Cardiology, Duke University Medical Center, Durham, North Carolina 27710, [4]Saint Louis University, School of Medicine, Department of Otolaryngology, Head-Neck Surgery, St. Louis, Missouri 63110, and [5]Department of Internal Medicine, Division of Cardiology, University of California, Davis, California 95616, [6]Northern California, Health Care System, Mather, California 95655

**Spiral ganglion neurons (SGNs) of the eighth nerve serve as the bridge between hair cells and the cochlear nucleus. Hair cells use $Ca_v1.3$ as the primary channel for $Ca^{2+}$ inflow to mediate transmitter release. In contrast, SGNs are equipped with multiple $Ca^{2+}$ channels to mediate $Ca^{2+}$-dependent functions. We examined directly the role of $Ca_v1.3$ channels in SGNs using $Ca_v1.3$-deficient mice ($Ca_v1.3^{-/-}$). We revealed a surprising finding that SGNs functionally express the cardiac-specific $Ca_v1.2$, as well as neuronal $Ca_v1.3$ channels. We show that evoked action potentials recorded from SGNs show a significant decrease in the frequency of firing in $Ca_v1.3^{-/-}$ mice compared with wild-type ($Ca_v1.3^{+/+}$) littermates. Although $Ca_v1.3$ is the designated L-type channel in neurons, whole-cell currents recorded in isolated SGNs from $Ca_v1.3^{-/-}$ mice showed a surprising remnant current with sensitivity toward the dihydropyridine (DHP) agonist and antagonist, and a depolarization shift in the voltage-dependent activation compared with that in the $Ca_v1.3^{+/+}$ mice. Indeed, direct measurement of the elementary properties of $Ca^{2+}$ channels, in $Ca_v1.3^{+/+}$ neurons, confirmed the existence of two DHP-sensitive single-channel currents, with distinct open probabilities and conductances. We demonstrate that the DHP-sensitive current in $Ca_v1.3^{-/-}$ mice is derived from $Ca_v1.2$ channel activity, providing for the first time, to our knowledge, functional data for the expression of $Ca_v1.2$ currents in neurons. Finally, using shRNA gene knockdown methodology, and histological analyses of SGNs from $Ca_v1.2^{+/-}$ and $Ca_v1.3^{+/-}$ mice, we were able to establish the differential roles of $Ca_v1.2$ and $Ca_v1.3$ in SGNs.**

*Key words:* **action potentials; calcium channels; deafness; hearing; neuronal degeneration; neuronal survival**

## Introduction

One of the captivating aspects of $Ca^{2+}$ regulation and function in neurons is the ability to partition $Ca^{2+}$-mediated proceedings for distinct $Ca^{2+}$ channels and domains. $Ca^{2+}$ inflow through diverse subtypes of $Ca^{2+}$ channels ($Ca_v$), e.g., $Ca_v2.1$ (P/Q-type) at neuromuscular junctions and most synapses in the CNS (Wheeler et al., 1994; Dunlap et al., 1995) and $Ca_v2.2$ (N-type) in the autonomic nervous system and some neurons in the CNS (Olivera et al., 1994; Poncer et al., 1997), trigger neurotransmitter release to induce short-term synaptic plasticity (Borst and Sakmann, 1998; Xu and Wu, 2005; Mochida et al., 2008). Upon exit from the intracellular orifice of $Ca_v2.1$ and 1.2 (cardiac isoform of L-type) channels, $Ca^{2+}$ ions bind to calmodulin, which is constitutively bound to the channel, and are partitioned into local domains, thus allowing swift $Ca^{2+}$ signaling, and global domains to promote the integration of $Ca^{2+}$ signaling at the whole-cell level (Imredy and Yue, 1992, 1994; Chaudhuri et al., 2005; Tadross et al., 2008). Even more fascinating is the revelation that a fragment of the C termini of $Ca_v1.2$ serves as a transcription factor (Gomez-Ospina et al., 2006), promoting neuronal survival and dendritic arborization to mediate long-term plasticity (West et al., 2001). It is unclear whether the presumed $Ca_v1.2$ in neurons is conductive. Since $Ca_v1.2$ and 1.3 (neuronal L-type channel) have similar pharmacology (Bean, 1984; Bell et al., 2001), it is difficult to distinguish the functionality of the two isoforms, although differences in their voltage-dependent activation

Received Dec. 28, 2013; revised March 20, 2014; accepted March 25, 2014.

Author contributions: N.C. and E.N.Y. designed research; P.L., H.J.K., J.-H.L., C.-R.S., S.G.F., A.M.-N., W.W., H.-G.W., M.A.G., and X.-D.Z. performed research; H.J.K., J.-H.L., K.J.D., and N.C. contributed unpublished reagents/analytic tools; P.L., H.J.K., J.-H.L., C.-R.S., W.W., X.-D.Z., and E.N.Y. analyzed data; M.A.G. and E.N.Y. wrote the paper.

This work was supported by grants to E.N.Y. from the National Institutes of Health (DC003,826). P.L. was funded by the National Organization for Hearing Research and National Natural Science Foundation of China (81200746). X.-D.Z was partially supported by AHA Western States Affiliate Beginning Grant-in-Aid (14BGIAA18870087). N.C. was funded by Grants HL085727, HL085844 and VA Merit Review Grant I01 BX000576. We thank members of our laboratory for comments on this manuscript. We thank Dr. Geoffrey S. Pitt for providing the $Ca_v1.2^{+/-}$ and their littermate control mice.

The authors declare no competing financial interests.

Correspondence should be addressed to Ebenezer N. Yamoah, Program in Communication Science, Center for Neuroscience, 1544 Newton Court, Davis, CA 95618. E-mail: enyamoah@ucdavis.edu.

DOI:10.1523/JNEUROSCI.5416-13.2014

 0270-6474/14/347383-11$15.00/0

and functions have been noted (Xu and Lipscombe, 2001; Zhang et al., 2002).

Similarly, inflowing $Ca^{2+}$ ions through multiple $Ca_v$ channels in auditory neurons represent the prevailing trigger of neurotransmitter release at the cochlear nucleus and spiral ganglion neuron (SGN) firing phenotypes (Chen et al., 2011; Lv et al., 2012), thereby orchestrating peripheral auditory information coding (Trussell, 1997; Cao and Oertel, 2010; Howard and Rubel, 2010; Rutherford et al., 2012). For long-term structural changes and growth, $Ca^{2+}$ influx through L-type channels promotes SGN survival *in vitro* (Hegarty et al., 1997). Of significant application and pragmatic ramifications, *in vivo*, is the finding that direct electrical stimulation of SGNs increases SGN survival (Mitchell et al., 1997; Leake et al., 1999). Conversely, excessive $Ca^{2+}$ inhibits neural outgrowth (Roehm et al., 2008), raising the possibility that a window of intracellular $Ca^{2+}$ activity is required for long-term plasticity in auditory neurons. The $Ca_v$ mediating SGN growth and survival and the mechanisms remain unspecified.

Here, we construed that a direct strategy to disentangle the roles of L-type channels in SGNs is to examine their functional properties from *$Ca_v1.3$*-null mutant (*$Ca_v1.3^{-/-}$*) mice (Platzer et al., 2000; Dou et al., 2004). We show that *$Ca_v1.3^{-/-}$* SGNs remain sensitive to dihydropyridine (DHP) compounds. Moreover, the residual DHP-sensitive current had ~10 mV depolarized shift in voltage-dependent activation properties. Direct measurement of channel activity showed two independent DHP-sensitive unitary conductances and distinct open probabilities. We have proceeded further in determining the differential roles of the DHP-sensitive currents in SGNs.

## Materials and Methods

The animal protocol for this study was approved by the Institutional Animal Care and Use Committee of the University of California, Davis. We used 1- to 4-month-old *$Ca_v1.2^{+/-}$*, *$Ca_v1.3^{-/-}$*, *$Ca_v1.3^{+/-}$*, and their wild-type (WT) C57BL/6J littermate control mice. We used only *$Ca_v1.2^{+/-}$* and their WT littermates because the *$Ca_v1.2^{-/-}$* mice are not viable.

*Isolation of SGNs.* SGNs were isolated from male and female mouse inner ears as described previously (Lv et al., 2010, 2012). Briefly, mice were killed and the temporal bones were removed in a solution containing Minimum Essential Medium with Hank's salt (Invitrogen), 0.2 g/L kynurenic acid, 10 mM $MgCl_2$, 2% FBS (v/v), and 6 g/L glucose. The SGN tissue was dissected and split into three equal segments: apical, middle, and basal across the modiolar axis. We used the apical and basal thirds to ensure an adequate, viable neuronal yield for the experiments (Lv et al., 2010). Additionally, we pooled tissue from three mice into each SGN culture. The apical and basal tissues were digested separately in an enzyme mixture containing collagenase type I (1 mg/ml) and DNase (1 mg/ml) at 37°C for 20 min. After a series of gentle triturations and centrifugation in 0.45 M sucrose, the cell pellets were reconstituted in 900 ml of culture media [Neurobasal-A, supplemented with 2% B27 (v/v), 0.5 mM L-glutamine, 100 U/ml penicillin; Invitrogen] and filtered through a 40 $\mu$m cell strainer for cell culture. We cultured SGNs for ~24–48 h to allow detachment of Schwann cells from neuronal membrane surfaces. We used strict electrophysiological criteria, described previously (Lv et al., 2010), to govern the quality of acceptable data. All electrophysiological experiments were performed at room temperature (21−22°C). Reagents were obtained from Sigma-Aldrich, unless otherwise specified.

*Current- and voltage-clamp experiments.* Current-clamp configuration was used to record action potentials (APs). Extracellular solution for most experiments contained the following (in mM): 145 NaCl, 6 KCl, 1 $MgCl_2$, 0–2 $CaCl_2$, 10 D-glucose, and 10 HEPES, at pH 7.3. For perforated patch experiments, the tips of the pipettes were filled with the internal solution containing the following (in mM): 150 KCl, 10 HEPES, and 10 D-glucose, at pH 7.3. The pipettes were front filled with the internal solution and back filled with similar solution containing 250 $\mu$g/ml amphotericin and 2 mM $Ca^{2+}$. Thus, a switch from perforated patch to whole-cell mode results in rapid cell death.

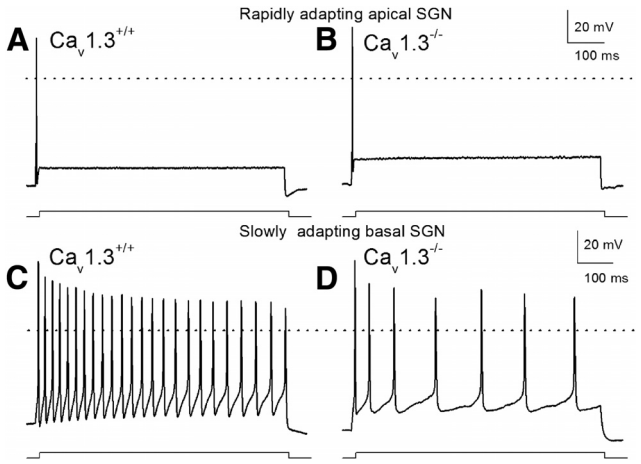


**Figure 1.** Evoked APs recorded from *$Ca_v1.3$*-null mutant mice show a decreased firing frequency and increased AP duration in slowly, but not rapidly, adapting SGNs. ***A***, Representative recordings from WT (*$Ca_v1.3^{+/+}$*) and (***B***) homozygous (*$Ca_v1.3^{-/-}$*) mutant mice. We used the perforated-patch configuration to evoke electrical activity from isolated 3- to 4-month-old SGNs. Evoked APs were elicited with a 0.1 nA current (see stimulation protocol below each voltage trace) for a duration of ~700 ms from rapidly (***A***, ***B***) and slowly (***C***, ***D***) adapting SGNs in a bath solution containing 2 mM $Ca^{2+}$. The dashed lines show 0 mV levels. Analyses of AP properties showed significant changes ($p < 0.05$) in rmp, spike latency, frequency, and duration in slowly adapting SGNs in *$Ca_v1.3^{-/-}$* compared with *$Ca_v1.3^{+/+}$* mice (see Table 1 for summary data). In contrast, alterations in AP properties of rapidly adapting SGNs were not statistically significant.

Whole-cell and cell-attached, single-channel voltage-clamp recordings of $Ca^{2+}/Ba^{2+}$ currents were performed using an Axopatch 200B amplifier (Molecular Devices). Current traces were amplified, filtered (bandpass 2–10 kHz), and digitized at 5–500 kHz using an analog-to-digital convertor, Digidata 1200 (Molecular Devices) as described earlier (Levic et al., 2007; Rodriguez-Contreras et al., 2008). Electrodes (2–3 MΩ) were pulled from borosilicate glass and the tips were fire polished. The electrodes contained the following (in mM): 70 CsCl, 70 *N*-methyl-D-glucamine (NMDG), 1 $MgCl_2$, 10 HEPES, 2–5 EGTA, 1 $CaCl_2$, and 4 $Cs_2ATP$, at pH 7.2 with CsOH. The bath solution was constantly perfused (~2–3 ml/min) and contained the following (in mM): 120 Choline chloride, 20 TEACl, 5 4-AP, 0.02 linopirdine, 2 CsCl, 1.8–5 $CaCl_2$, 0.5 $MgCl_2$, 10 HEPES, and 5 D-glucose, at pH 7.4 with NaOH. In all cases, the $Ca^{2+}$ concentration was adjusted with $Mg^{2+}$. Inward $Ca^{2+}$ current traces were generated with depolarizing voltage steps from a holding potential of −100 to −40 mV and stepped to varying positive potentials ($\Delta V$ = 5–10 mV). The capacitative transients were used to estimate the capacitance of the cell, as an indirect measure of cell size. The seal resistance was typically 10–15 GΩ. Currents were measured with capacitance and series resistance compensation (>90%), filtered at 2 kHz using an 8-pole Bessel filter, and sampled at 5 kHz. Given that the maximum current recorded was < 1 nA, the expected voltage error was < 1.5 mV. The series resistance was monitored during the course of the experiments. The liquid junction potentials were measured (<3 mV) and corrected.

Whole-cell $Ca^{2+}$ current amplitudes at varying test potentials were measured at the peak and steady-state levels using a peak and steady-state detection routine; the current magnitude was divided by the cell capacitance (pF) to generate the current density–voltage relationship. The stock solutions of all channel blockers and agonists were made either in $ddH_2O$ or DMSO and stored at −20°C. The final concentration of DMSO in the recording bath solution was ~0.0001%. This concentration of DMSO had no effect on APs and did not alter $Ca^{2+}$ current recordings (data not shown).

The standard configurations for cell-attached, single-channel recordings of the patch-clamp techniques (Hamill et al., 1981) were used to

**Table 1. Changes in membrane properties after null deletion of *$Ca_v1.3$***

| | Apex | | | | | Base | | | | |
|---|---|---|---|---|---|---|---|---|---|---|
| | Latency (ms) | rmp (mV) | Duration (ms) | Half-width (ms) | Spike # | Latency (ms) | rmp (mV) | Duration (ms) | Half-width (ms) | Spike #/s |
| $Ca_v1.3^{+/+}$ | 3.1 ± 0.3 | −64.6 ± 1.7 | 5.5 ± 0.7 | 0.52 ± 0.08 | 1 | 7.1 ± 1.4 | −59.3 ± 4.2 | 10.0 ± 1.7 | 0.81 ± 0.15 | 37.7 ± 12.6 |
| $Ca_v1.3^{-/-}$ | 3.1 ± 0.6 | −67 ± 4.1 | 5.8 ± 1.4 | 0.66 ± 0.26 | 1 | 11.6 ± 3.2** | −65.4 ± 4.5** | 15.1 ± 3.6** | 0.78 ± 0.19 | 12.1 ± 7.4** |

*$p < 0.05$; **$p < 0.01$. Apex: $Ca_v1.3^{+/+}$ ($n = 9$), $Ca_v1.3^{-/-}$ ($n = 9$); base: $Ca_v1.3^{+/+}$ ($n = 12$), $Ca_v1.3^{-/-}$ ($n = 7$).

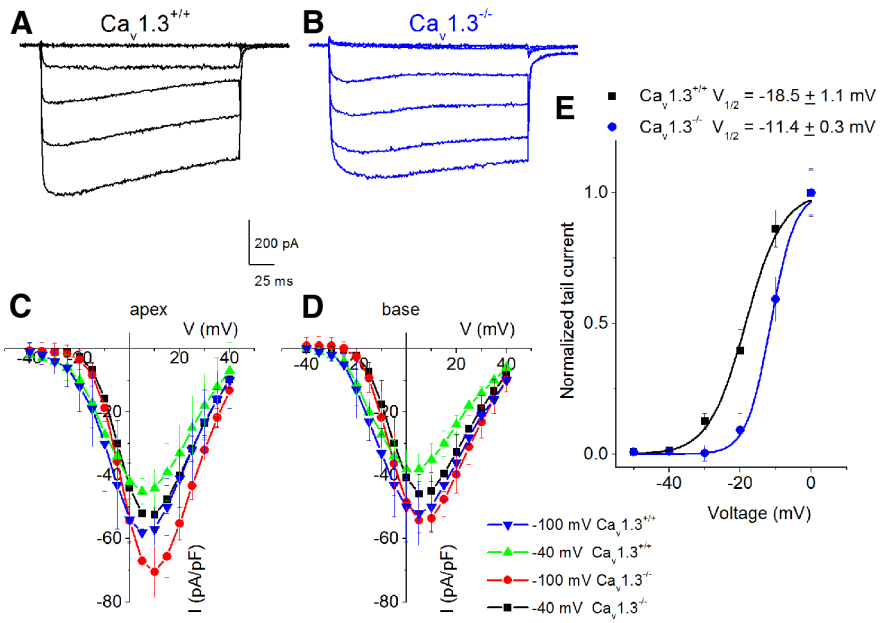


**Figure 2.** Whole-cell $Ca^{2+}$ currents in $Ca_v1.3^{+/+}$ and $Ca_v1.3^{-/-}$ SGNs demonstrate substantial differences in the activation properties. ***A***, A family of membrane $Ca^{2+}$ current traces recorded from SGNs isolated from $Ca_v1.3^{+/+}$ mice, using 2 mM external $Ca^{2+}$ as the charge carrier. Inward $Ca^{2+}$ currents were generated using depolarizing test voltages from −50 to 40 mV, in 5 mV increments from a holding voltage of −40 mV. For clarity, some of the traces were omitted in the illustration. Outward $K^+$ currents were suppressed with a bath solution containing TEA, 4-AP, and internal solution containing $Cs^+$ and $NMG^+$ (see Materials and Methods). ***B***, The current traces were recorded as in ***A***, from a holding voltage of −40 mV using $Ca_v1.3^{-/-}$ SGNs (blue). ***C***, ***D***, Summary of the corresponding current–density–voltage (I–V) relations for recording at −100 and −40 mV holding voltages, using apical (***C***) and basal (***D***) $Ca_v1.3^{+/+}$ and $Ca_v1.3^{-/-}$ SGNs. Data were summarized from $n = 9$. The current densities for $Ca_v1.3^{+/+}$ and $Ca_v1.3^{-/-}$ apical and basal neurons were similar, except when cells were held at −100 mV. At this holding voltage, the current density for apical neurons was significantly greater than basal neurons. The peak current density (pA/pF) for apical neurons at a holding potential of −100 mV = −70.5 ± 8.0; and basal neurons = −54.7 ± 3.9 ($n = 9$), $p < 0.01$. ***E***, Neurons were held at a holding potential of −50 mV and tail currents were generated at −20 mV, and the steady-state voltage dependence of activation was plotted and fitted with a first order Boltzmann function for $Ca^{2+}$ currents derived from $Ca_v1.3^{+/+}$ and $Ca_v1.3^{-/-}$ (blue) basal neurons. The half-activation voltages ($V_{1/2}$, in mV) were −18.5 ± 1.1 and −11.4 ± 0.3, and the maximum slope factors ($k$, in mV) were 7.0 ± 1.5 and 9.1 ± 2.6. ($n = 7$).

record single $Ca^{2+}$ channel currents. Patch electrodes were pulled from borosilicate glass capillaries with a Flaming/Brown micropipette puller (P-97; Sutter Instruments), and coated with Sylgard 184 (Dow Corning) to within 100 μm from the tip and fire polished before use. Single-channel recordings of membrane patches were held at −70/−50 mV, and stepped to different depolarizing test pulses at frequencies between 0.2 and 0.5 Hz. Current traces were amplified and filtered using an 8-pole Bessel filter at 2 kHz, and digitized at 10 kHz using custom-written software. Patch electrodes were filled with a $Ba^{2+}$ solution (50 mM) containing the following (in mM): 20 NMDG, 20 TEACl, 5 4-AP, and 5 HEPES, at pH 7.4 (adjusted with TEAOH). The osmolarity of the patch-electrode solution was ~290 mOsmol. Stock solutions of Bay K 8644 and nimodipine (100 mM) were made in DMSO, and a final concentration of 5 μM was used. The bath solution contained the following (in mM): 80 KCl, 3 D-glucose, 20 TEACl, 0.5 $CaCl_2$, 5 4-AP, and 5 HEPES, at pH 7.4 with TEAOH, to shift the resting potential to ~0 mV (Rodriguez-Contreras et al., 2002; Rodríguez-Contreras and Yamoah, 2003). The $Ca^{2+}$ channel blockers nimodipine (L-type), ω-conotoxin GVIA (CTX; N-type), ω-agatoxin IVA (ATX; P/Q-type), ω-theraphotoxin-Hg1a, ω-TRTX-Hg1a (rSNX-482; R-type; Alomone Labs), and mibefradil (T-type) were bath applied for whole-cell and single-channel recordings. In all cases, liquid junction potentials were measured and corrected as described previously (Rodriguez-Contreras and Yamoah, 2001).

For single-channel recordings, leakage and capacitative transient currents were subtracted by fitting a smooth template to null traces. Leak-subtracted current recordings were idealized using a half-height criterion. Transitions between closed and open levels were determined by using a threshold detection algorithm, which required that two data points exist above the half-mean amplitude of the single-unit opening. The computer-detected openings were confirmed by visual inspection, and sweeps with excessive noise were discarded. Amplitude histograms at a given test potential were generated, and then fitted to a single Gaussian distribution using a Levenberg–Marquardt algorithm to obtain the mean and SD. At least four voltage steps and their corresponding single-channel currents were used to determine the unitary conductance. Single-channel current–voltage relations were fitted by linear least-square regression lines and single-channel conductances obtained from the slope of the regression lines. Curve fits and data analyses were performed using Origin software (MicroCal). Where appropriate, we present data in the form of mean ± SD. Significant differences between groups were tested using paired/unpaired Student's $t$ test with a significance of $p < 0.05$.

*Immunocytochemistry.* SGNs were isolated from the mouse inner ear and cultured for 48 h as described previously (Wei et al., 2007; Lv et al., 2010). Neurons were fixed for 30 min with 2% paraformaldehyde in PBS, washed, and then permeabilized in 0.5% Triton X-100 in PBS for 5 min. The samples were incubated for 1 h in a blocking solution containing PBS, 1% horse serum in PBS, followed by 3–5 h incubation with $Ca^{2+}$ channel antibodies against $Ca_v1.2$, residues 865–881, and $Ca_v1.3$, residues 859–875 (Alomone Labs; Abcam), at 1:100 to 1:500 dilutions. To identify neurons, samples were counterstained with an antibody against the neuronal marker TUJ1 as described previously (Wei et al., 2008). Cells were then incubated with appropriate secondary antibodies for 2 h, washed, mounted using antifade mounting medium, and viewed with a Zeiss LSM 510 confocal microscope.

For immunohistochemistry of cochlear tissues, sedated (Avertin; 2,2,2-tribromoethanol); 300 μg/gm body weight, i.p.) mice were transcardially perfused with 10 ml of PBS, followed by 10 ml of 4% paraformaldehyde in PBS. The temporal bones were removed, and the cochlea was perfused via the oval and round windows. The temporal bones were then immersed in fixative for 60 min. After fixation, the cochleae were decalcified (120 mM EDTA, pH 7.0; 24 h; ~21°C). Cochleae were processed sequentially with 10 and 30% sucrose at 4°C overnight, then embedded in OTC for cryosection in the modiolar plane. Sections were

washed in PBS, permeabilized in 0.1% Triton X-100 for 25 min, and then incubated for 30 min in a blocking solution containing 1% bovine serum albumin and 1% goat serum. The 10 $\mu$m sections were incubated with primary antibody overnight at 4°C. The rinsed sections were then incubated (2 h; 4°C) in a fluorescent dye-conjugated secondary antibody. Images were captured with a Zeiss LSM 510 confocal microscope.

*Construction of siRNAs, expression vector for $Ca_v1.2$ and $Ca_v1.3$ knock down.* Four of 19 base-long siRNAs were designed, using siRNA at WHITEHEAD software for each gene, and cloned under U6 promoter in pSilencer5.1-U6 vector to produce hairpin siRNAs (shRNAs). Each shRNA expression clone was cotransfected into HEK 293 cells with $Ca_v1.2$ or $Ca_v1.3$ expression clones, incubated for ~72 h, and $Ca_v1.2$ or $Ca_v1.3$ expression was determined by immunostaining and patch-clamp recordings of $Ca^{2+}$ currents. The most efficient shRNA (>90% reduced protein expression level compared with control) among the four was chosen and used. shRNA sequence for $Ca_v1.2$ is 5′-**TGGAAACCATTTGAAATCA**TTCAAGAG**ATGATTTCAAATGGTTTCCA**TTTTT, and for $Ca_v1.3$ is 5′-**GTAGAATATGCCTTCCTGA**TTCAAGAGA**TCAGGAAGGCATATTCTAC**TTTTT (sense and antisense strands are bold and loops are underlined).

*Terminal dUTP nick end labeling (TUNEL) assay.* After 7 d in culture, SGNs that were transfected with scrambled shRNA, C3-shRNA to knockdown $Ca_v1.2$, and D2-shRNA to knockdown $Ca_v1.3$ were fixed in 4% paraformaldehyde for 20 min, washed 3× in PBS, and postfixed in ethanol/acetic acid (2:1) for 5 min. Following two washes in PBS, a 50 $\mu$l TUNEL reaction mixture (*in situ* cell death detection fluorescein; Roche Applied Science) was added and incubated in the dark and humidified chamber for ~2 h at 37°C. The specimens were washed 3× in PBS, counterstained with 4′,6-diamidino-2-phenylindole·2HCl (DAPI), mounted, and viewed under a Zeiss LSM 510 confocal microscope.

*Cochlear histology.* Animals were anesthetized (Avertin), 300 $\mu$g/gm BW, i.p.) and transcardially perfused with PBS (5 ml, 23°C), followed by a solution of 4% paraformaldehyde and 2% glutaraldehyde in 0.1 M PBS (10 ml, pH 7.4, 23°C). The temporal bones were removed and opened to expose the otic capsule. The stapes was removed and a perforation was made in the round window, following which fixative was perfused through the oval window. The bulla was then immersed in fixative (12 h, 4°C), rinsed with PBS, postfixed (1% OsO4 in 0.1 M PBS, 30 min), and decalcified (80 ml, 120 mM, 2SS EDTA, 23°C). The cochleae were dehydrated through a graded series of ethanol and propylene oxide before infiltration and embedding in plastic resin (EmBed 812; EMS). After polymerization (12 h, 58°C), the cochlea was bisected. The half-cochleae were re-embedded and completely polymerized (18 h, 58°C). Semithick sections (1 $\mu$m) with a modiolar orientation were cut and stained with toluidine blue for examination using a compound microscope (Zeiss or Nikon eclipse 80i) interfaced with a digital camera and an image analysis system (AxioVision from Zeiss or NIS Elements from Nikon). Images were adjusted using Adobe Photoshop according to the guidelines of the Microscopy Society of America.

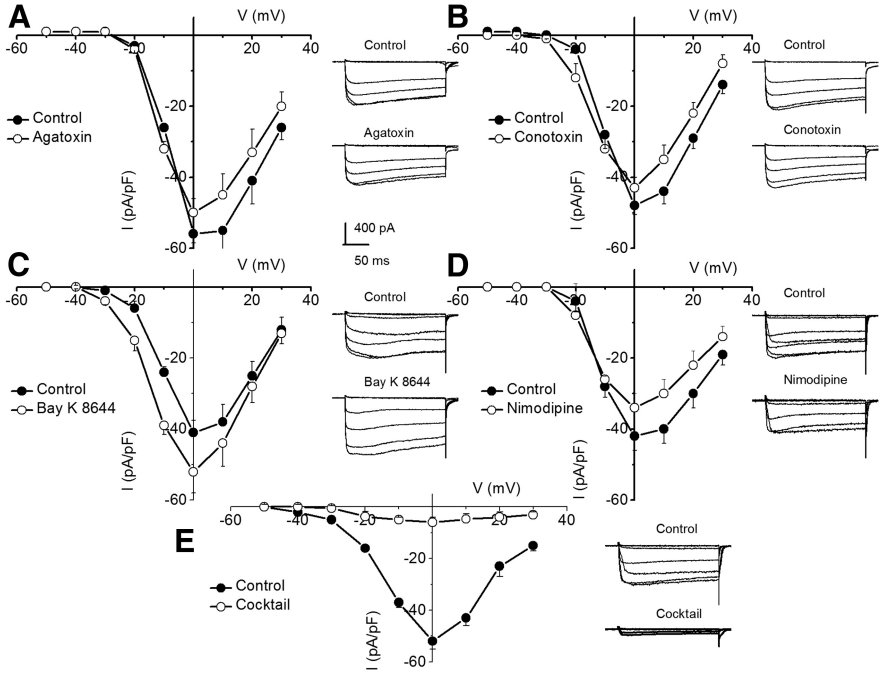


**Figure 3.** Pharmacological characterization of $Ca^{2+}$ currents in $Ca_v1.3^{-/-}$ basal SGNs. $Ca^{2+}$ currents from basal SGNs were generated using a holding voltage of −50 mV and stepped to depolarizing voltage steps from −50 to 30 mV, using a $\Delta V$ of 10 mV. The *I–V* relations were generated before (●) and after (○) application of $Ca^{2+}$ current blockers, $\omega$-agatoxin IVA for P/Q-type (***A***), $\omega$-conotoxin MVIIA for N-type (***B***) currents. ***A***, *I–V* relations for control and the remaining current density after application of 1 $\mu$M $\omega$-agatoxin IVA ($n = 7$). Insets to the right of the plots are representative current traces used to generate the *I–V* curves. ***B***, Similar experiments and *I–V* curves as described in ***A***, to determine the component of the whole-cell $Ca^{2+}$ current that was derived from N-type channels ($n = 7$). We applied 1 $\mu$M conotoxin MVIIA in these sets of experiments. ***C***, Despite null deletion of the reported neuronal L-type $Ca^{2+}$ channel, $Ca_v1.3$, whole-cell $Ca^{2+}$ currents in $Ca_v1.3^{-/-}$ neurons remained sensitive to the DHP agonist, Bay K 8644 (5 $\mu$M). The $Ca^{2+}$ current was increased by ~1.25-fold ($n = 7$). ***D***, Consistent with the expression of an additional L-type current in the whole-cell $Ca^{2+}$ current from $Ca_v1.3^{-/-}$ SGNs, the current was suppressed by nimodipine (5 $\mu$M). ***E***, Summary *I–V* of the effect of a mixture (cocktail) of $Ca^{2+}$ channel blockers consisting of 5 $\mu$M nimodipine, 1 $\mu$M $\omega$-agatoxin IVA, 1 $\mu$M conotoxin MVIIA, and 200 nM rSNX-482 (R-type $Ca^{2+}$ channel blocker). Table 2 provides a summary of the proportion of currents that were sensitive to a specific $Ca^{2+}$ channel blocker.

frequency, AP duration, and latency in slowly adapting basal SGNs. In stark contrast, the AP properties were unscathed in rapidly adapting apical SGNs in $Ca_v1.3^{-/-}$ mice compared with their WT controls ($Ca_v1.3^{+/+}$; Fig. 1). The summary data ($n = 9$) from each group are shown in Table 1. Significant membrane hyperpolarization, prolongation of AP duration, latency, and spike numbers ($p < 0.01$) were observed in slowly adapting basal $Ca_v1.3^{-/-}$ neurons. These differences may represent intrinsic alterations in the membrane properties of SGNs.

## Results

### $Ca_v1.3^{-/-}$ SGNs have an altered firing pattern

We were able to demonstrate that null deletion of $Ca_v1.3$ had a severe impact on the resting membrane potential (rmp), spike

### Changes in whole-cell $Ca^{2+}$ current properties in $Ca_v1.3^{+/+}$ and $Ca_v1.3^{-/-}$ SGNs

We compared whole-cell $Ca^{2+}$ currents from SGNs derived from $Ca_v1.3^{+/+}$ and $Ca_v1.3^{-/-}$ mice at two distinct locations of the cochlear axis. Isolated SGNs were held at a holding potential of −100/−40 mV and stepped to depolarizing voltages ($\Delta V = 5$–10 mV) ranging between −50 and 40 mV. Figure 2, *A* and *B*, represents a family of $Ca^{2+}$ current traces recorded from $Ca_v1.3^{+/+}$ and $Ca_v1.3^{-/-}$ SGNs, respectively. As depicted in the whole-cell $Ca^{2+}$ current–density voltage relationships, the current densities between the $Ca_v1.3^{+/+}$ and $Ca_v1.3^{-/-}$, as well as apical (Fig. 2*C*) and basal (Fig. 2*D*) neurons, were comparable. The only exception between apical and basal SGNs occurred in the $Ca_v1.3^{-/-}$ neurons when held at a holding potential of −100 mV (e.g., the peak current density in pA/pF). Under this condition, apical neurons demonstrated a peak current density = −70.5 ± 8.0; ($n$ =

**Table 2. Percentage of $Ca^{2+}$ current blocked by different blockers at 0 mV step voltage after null deletion of *$Ca_v1.3$***

| | L-type Nimodipine 10 $\mu$M | P/Q-type $\omega$-Agatoxin IVA 1 $\mu$M | N-type Conotoxin MVIIA 1 $\mu$M | R-type rSNX-482 200 nM | Total Mixture |
|---|---|---|---|---|---|
| Apex | 24.6 ± 3.8% | 25.6 ± 3.3% | 22.3 ± 2.6% | 16.8 ± 6.2% | 86.6 ± 7.8% |
| Base | 15.6 ± 6.1%* | 29.9 ± 7.2% | 16.6 ± 5.1%* | 18.1 ± 6.5% | 82.1 ± 7.1% |

*$p < 0.05$ (apex vs base; $n = 7$).

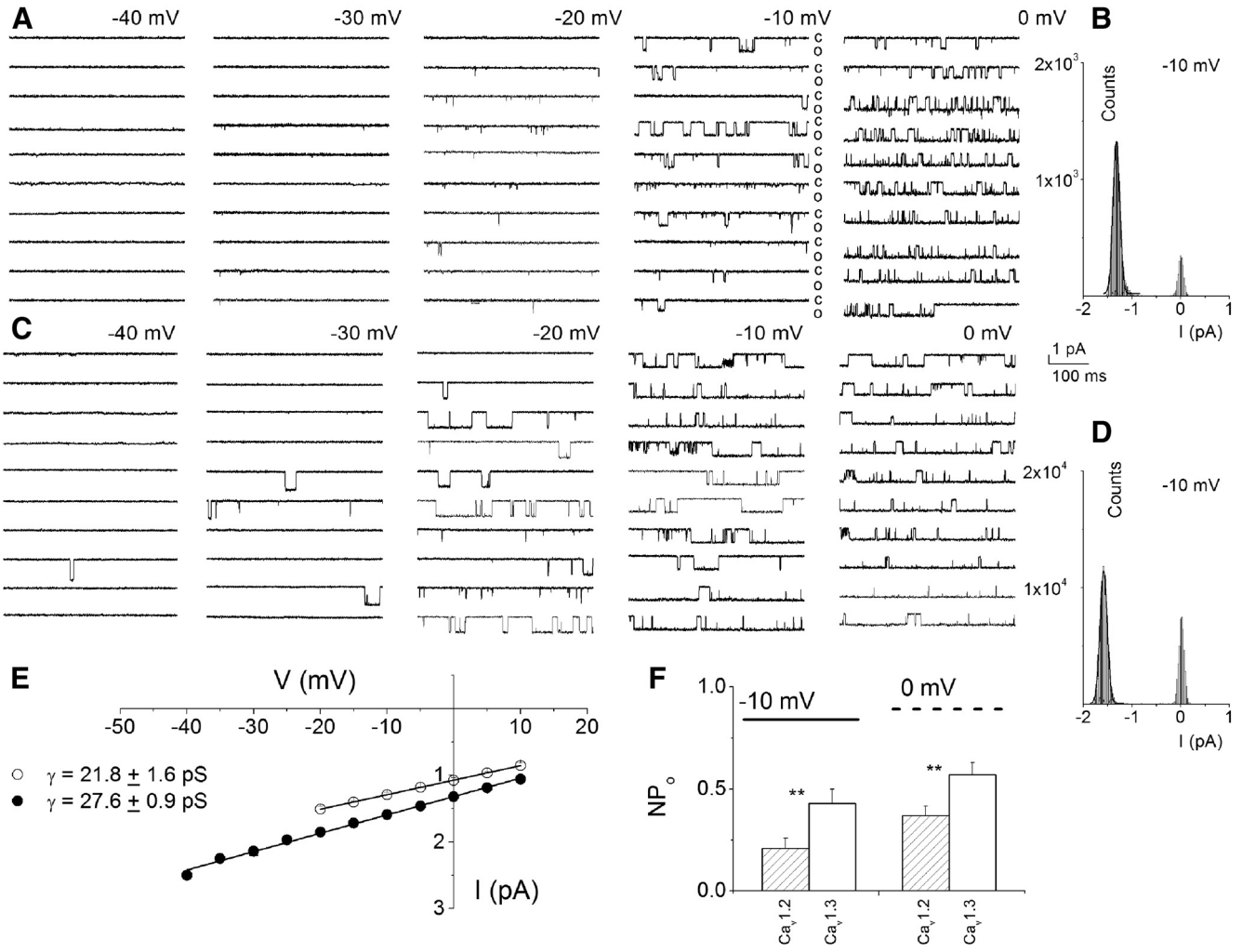


**Figure 4.** Two distinct Bay K 8644-sensitive unitary $Ba^{2+}$ currents in WT SGNs. ***A***, Ten consecutive single-channel traces of $Ba^{2+}$ currents at test potentials from −40 to 0 mV were obtained from L-type channels using the agonist, Bay K 8644 (5 $\mu$M), in the bath solution. The experiments were performed first in the absence of Bay K 8644. After tight seal cell-attached configuration was established, we examined characteristic L-type channel brief openings, before bath application of 5 $\mu$M Bay K 8644 containing solution. Patches with single channels that were not sensitive to the Bay K 8644 were discarded. Single-channel $Ba^{2+}$ current traces were recorded using 50 mM $Ba^{2+}$ as the charge carrier. The traces were generated by holding the membrane patch at −50 mV and stepping to potentials indicated above each set of traces. The open (O) and closed (C) levels are indicated. Brief openings were predominant in the unmodified channel (data not shown). ***B***, An example of amplitude histogram used to determine the mean magnitude of unitary currents at −10 mV step potential (~1.3 pA) is shown. We denote this channel as $Ca_v1.2$. ***C***, A family of 10 consecutive traces, as illustrated in ***A***, obtained from another distinct Bay K 8644-sensitive channel. Openings of this distinct channel could be seen at more negative voltages than the channel in ***A***. The channel is ascribed as $Ca_v1.3$. ***D***, Amplitude histogram of the putative $Ca_v1.3$ at −10 mV step voltage. ***E***, Single-channel conductance ($\gamma$) of two distinct L-type channels in SGNs were determined using linear least-square fits to the mean single-channel amplitude ($Ca_v1.2$, ○; $Ca_v1.3$, ●) at different step potentials. The conductance of the L-type channels: $Ca_v1.2 = 21.8 \pm 1.6$ pS ($n = 7$) and $Ca_v1.3 = 27.6 \pm 0.9$ pS ($n = 7$). ***F***, Summary histogram of the open probability ($NP_o$) of $Ca_v1.2$ and $Ca_v1.3$ at the test potentials (−10 mV, solid line) and (0 mV, dashed line); $^{**}p < 0.01$.

9), while in basal neurons, the peak current density = −54.7 ± 3.9 ($n = 9$, $p < 0.01$). $Ca^{2+}$ currents were activated from a holding potential of −50 mV and the steady-state activation with respect to voltage derived from the tail currents at −20 mV were fitted with a Boltzmann function. The half-activation voltage ($V_{1/2}$) was −18.5 ± 1.1 mV ($n = 7$) for *$Ca_v1.3^{+/+}$* and −11.4 ± 0.3 ($n = 7$) for *$Ca_v1.3^{-/-}$* SGNs. The ~7 mV rightward shift in the $V_{1/2}$ for $Ca^{2+}$ currents is consistent with the low-voltage activation properties of the $Ca_v1.3$ current (Rodriguez-Contreras and Yamoah, 2001; Xu and Lipscombe, 2001; Zhang et al., 2002; Michna et al., 2003; Schnee and Ricci, 2003; Zampini et al., 2010). We determined the relative densities of high voltage-activated $Ca^{2+}$ currents derived from multiple channel subtypes in isolated SGNs from *$Ca_v1.3^{-/-}$* mice using pharmacologic strategies (Lv et al., 2012). To suppress low voltage-activated $Ca^{2+}$ currents, these subsequent experiments were performed at a holding voltage of −50 mV. Using ATX for P/Q-type, CTX for N-type, and rSNX-482 for R-type $Ca^{2+}$ currents, and in combination, we

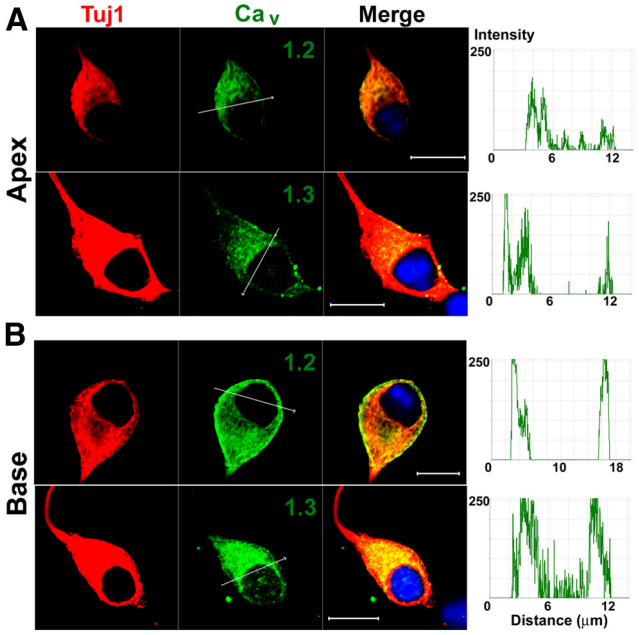


**Figure 5.** SGNs express $Ca_v1.2$ and $Ca_v1.3$ channels. Cultured (48 h) SGNs were fixed and labeled with antibodies against $Ca_v1.2$ and $Ca_v1.3$. Neurons were labeled with the neuronal marker, Tuj1 (red), the $Ca_v$ channels (green), and the nuclei were stained with DAPI (blue); the merged images are shown on the right. The graphs adjacent to the merged images describe the fluorescent intensity differences in the expression of the channel against distance marked with a white arrow on the plasma membrane and cytosol. ***A*** and ***B*** show expression of the two channels in apical and basal SGNs, respectively. Scale bar, 10 $\mu$m.

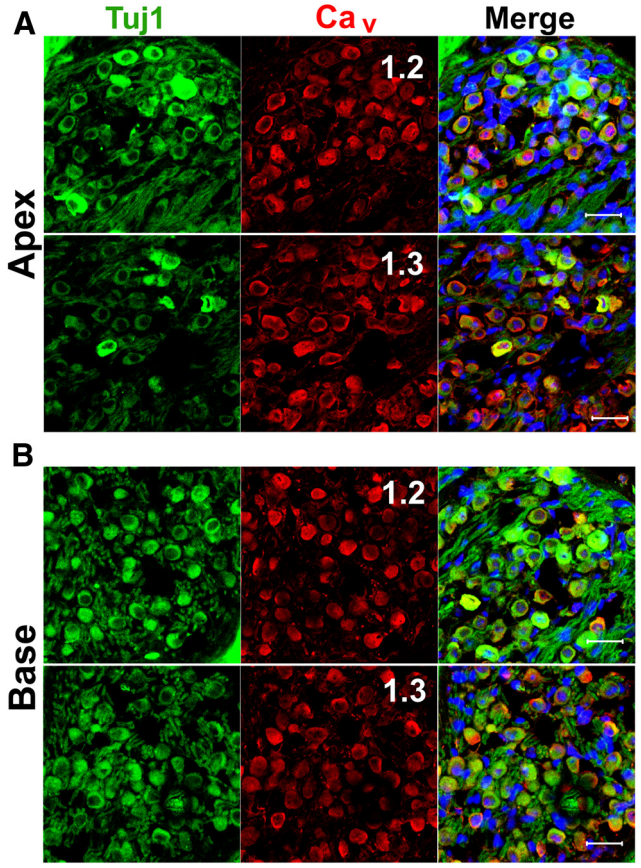


**Figure 6.** Expression of $Ca_v1.2$ and $Ca_v1.3$ in C57BL/6 mouse cochlear sections. ***A***, ***B***, Apical (***A***) and basal (***B***) SGNs expressed $Ca_v1.2$ and $Ca_v1.3$ *in vivo*. We performed immunolabeling, as described in Figure 5, on sections of the cochlea from 3-month-old mice. SGNs were labeled with antibodies against $Ca_v1.2$ and $Ca_v1.3$ (red). Neurons were labeled with the neuronal marker Tuj1 (green) and the nuclei were stained with DAPI (blue). SGNs stained positively to $Ca_v1.2$ and $Ca_v1.3$. Scale bar, 20 $\mu$m.

demonstrated that the $Ca_v1.3^{-/-}$ SGNs expressed multiple current subtypes in apical and basal neurons in relatively similar proportions as in $Ca_v1.3^{+/+}$ neurons (Lv et al., 2012; Fig. 3, Table 2).

Although it has been demonstrated in the $Ca_v1.3^{-/-}$ mouse model that the channel is nonfunctional in multiple tissues, such as pancreatic $\beta$-cells and heart and hair cells, resulting in diseased phenotypes including diabetes, bradycardia, and deafness (Namkung et al., 2001; Zhang et al., 2002; Dou et al., 2004), we cross-checked the possibility for expression of an additional L-type current in the SGNs. Application of two different DHP antagonists, nifedipine (10 $\mu$M) or nimodipine (5 $\mu$M), resulted in a significant reduction of whole-cell $Ca^{2+}$ currents from the isolated $Ca_v1.3^{-/-}$ SGNs (Fig. 3, Table 2). We confirmed the DHP-specificity by examining the effects of Bay K 8644, the DHP agonist. Consistent with the actions of DHPs on L-type currents, Bay K 8644 induced a leftward shift in the activation voltage of the $Ca^{2+}$ current by ~10 mV, suggesting that a remnant L-type current persisted after null deletion of $Ca_v1.3$. The findings may represent an upsurge of an otherwise latent $Ca_v1.2$ channel in WT SGNs. Thus, the presence of an apparent DHP-sensitive current in a genetically modified mouse model may not suffice to conclude that $Ca_v1.2$ is expressed in WT SGNs. The only known tangible difference in currents derived from $Ca_v1.2$ and $Ca_v1.3$ channels is that the latter activates at relatively negative voltages and is less sensitive to the DHPs (Xu and Lipscombe, 2001; Zhang et al., 2002).

### Elementary properties of $Ca_v1.2$ and $Ca_v1.3$ currents in SGNs

A more direct strategy to examine the channels that contribute to whole-cell currents is to record from single-channel patches in the cell-attached configuration. Figure 4*A* shows a family of single-channel $Ba^{2+}$ current traces recorded from a patch, obtained from a WT basal neuron, that was held at −50 mV holding

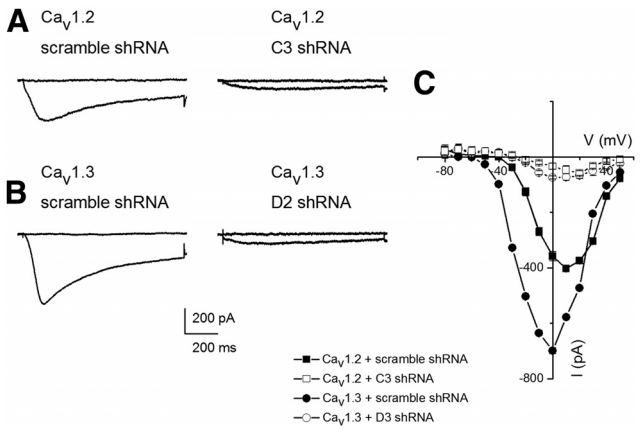


**Figure 7.** Assessment of efficiency of knockdown of $Ca_v1.2$ and $Ca_v1.3$ by shRNA in HEK 293 cells. ***A***, Representative whole-cell current traces were recorded from HEK 293 cells transfected with $Ca_v1.2$ DNA and scrambled shRNA as controls (left) and C3 shRNA (right). Recordings were made 96 h after transfection. ***B***, Similar recordings were made after transfecting scrambled shRNA with $Ca_v1.3$ DNA used as control experiments (left) and D2 shRNA (right). ***C***, Shown is the summary data of the current–voltage relationships for the experiments described in ***A*** and ***B***. Data were obtained from seven cells in each group.

potential and stepped to voltages indicated after application of external solution containing 5 $\mu$M Bay K 8644 (Fig. 4*A*,*C*). The charge carrier was 50 mM $Ba^{2+}$. Membrane depolarization resulted in typical brief and long openings. Moreover, long open-

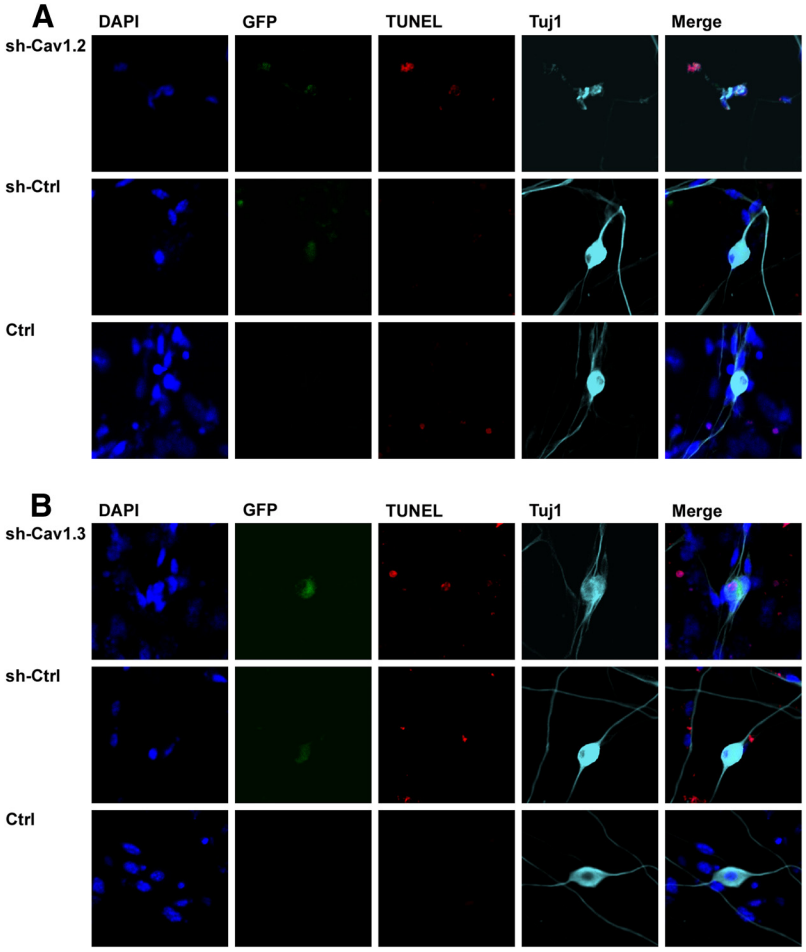


**Figure 8.** Assessment of apoptotic cell death. ***A***, Top, Shows cultured SGNs that were transfected with C3 shRNA to knockdown $Ca_v1.2$ channels. The leftmost column shows DAPI-stained nuclei (blue), while GFP (green) denotes the reporter gene in the second column from the left. The adjacent column shows TUNEL-positive apoptotic neurons (red), while the second column from the right depicts immunopositivity for the neuronal marker stain, Tuj1 (cyan). The column at the extreme right is the merged image. For C3 knockdown of *$Ca_v1.2$*, there were 1115 apoptotic neurons from a total of 1163 neurons (~96%). For scrambled shRNA controls, there were 78 apoptotic neurons from a total of 986 neurons (~8%). Cultures without addition of scrambled shRNA and C3 shRNA had 45 TUNEL-positive neurons out a total of 746 neurons (~6%). ***B***, Data obtained using D2 shRNA, to knockdown $Ca_v1.3$ channels, scrambled shRNA and without the addition of D2 and scrambled shRNA are illustrated here. In this experimental group, D2-mediated knockdown of *$Ca_v1.3$* resulted in 753 apoptotic neuronal deaths from a total of 846 neurons counted (~89%). For control scrambled shRNA culture, we counted 111 TUNEL-positive neurons among 1008 neurons (~11%), and cultures with no scrambled or D2 shRNA had 23 TUNEL-positive neurons in 563 neurons (~4%).

### Localization of $Ca_v1.2$ and $Ca_v1.3$ proteins in SGNs

To obtain biochemical evidence for the existence of $Ca_v1.2$ and $Ca_v1.3$ expression in SGNs, we used antibodies against the two channels. We observed positive labeling in the membrane and cytoplasm of SGNs in both apical and basal neurons (Fig. 5). Positive labeling of neuronal membrane was atypical in control experiments in which SGNs were pre-incubated with purified peptides supplied by the company (data not shown). To ensure that the data obtained from isolated neurons, *in vitro*, were consistent with *in vivo* conditions, we repeated the experiments using cochlear sections from age-matched WT littermates (Fig. 6), confirming the existence of $Ca_v1.2$ and $Ca_v1.3$ in adult SGNs. These findings were in keeping with previous reports demonstrating the expression of $Ca_v1.3$ in SGNs (Lv et al., 2012). Thus, biophysical and biochemical analyses divulged from these studies strongly suggest that $Ca_v1.2$ and $Ca_v1.3$ are functional components of $Ca^{2+}$ currents in SGNs.

### Altering the expression levels of $Ca_v1.2$ and $Ca_v1.3$ in SGNs to determine their functions

To assess the roles of $Ca_v1.2$ and $Ca_v1.3$ in SGNs, we designed shRNA to knock down the respective genes. As many as four different shRNA were designed and tested. The most efficient ones to knock down functional expression of the channels in a heterologous expression system (HEK 293 cells) were selected for $Ca_v1.2$ and $Ca_v1.3$ knockdown in SGNs. Shown in Figure 7, *A–C*, are the results from the knockdown of $Ca_v1.2$ and $Ca_v1.3$ after 72 h of transfection using C3 and D2, the respective nomenclature of the shRNA. Using magnetofectamine, we transfected shRNA into SGNs to knock down $Ca_v1.2$ and $Ca_v1.3$. The control groups were transfected with scrambled shRNA; the reporter gene was GFP. One week post-transfection, as many as 90–96% of all neurons that were transfected with GFP and C3 or D2 had undergone apoptotic cell death, as evaluated using TUNEL assay (Fig. 8*A*,*B*). The experiments were performed in triplicates of different culture preparations. The total number of neurons from the three different experiments is reported. For scrambled shRNA controls, there were 78 apoptotic neurons from a total of 986 neurons (~8%) counted. In the experimental groups using C3 to knock down *$Ca_v1.2$*, there were 1115 apoptotic neurons from a total of 1163 (~96%). Moreover, D2-mediated knockdown of *$Ca_v1.3$* resulted in 753 apoptotic neuronal deaths from a total of 846 neurons (~89%; Fig. 8). Functional confirmations of knockdown of *$Ca_v1.2$* and *$Ca_v1.3$* were difficult to assess since 7-d-old post-transfected neurons were not amenable to rigorous electrophysiological experiments.

ings were favored at more depolarized potentials. Visually, two-distinct DHP-sensitive, single-channel $Ba^{2+}$ currents were recorded from WT SGNs: (1) low voltage-activated current (activation voltage approximately −40 mV) with unitary current amplitude of approximately −1.6 pA and (2) high voltage-activated current (activation voltage approximately −20 mV) with amplitude of ~1.1 pA, at −10 mV step potential. The amplitude histograms obtained at a test potential of −10 mV are shown (Fig. 4*B*,*D*). Illustrated in Figure 4*E* are the summary data of the unitary current amplitudes plotted against the test potentials for the two distinct DHP-sensitive $Ca^{2+}$ channels. The slope conductances for the linear plots were 21.8 ± 1.6 pS ($n = 7$) and 27.6 ± 0.9 pS ($n = 7$). At specific voltages (−10, 0 mV), the large-conductance channel had open probabilities that were significantly greater than the small-conductance channel (Fig. 4*F*). For the patches we examined, we did not observe simultaneous recordings of the two L-type channels. However, it is conceivable that colocalization of the two L-type channels may occur in SGNs.

### $Ca_v1.2$ and $Ca_v1.3$ function in SGN survival

We reasoned that if $Ca_v1.2$ and $Ca_v1.3$ are necessary for the survival of SGNs, then reduced expression of these two genes is more likely to produce time-dependent alterations in neuronal survival. To test this hypothesis, we examined the extent of SGN survival in young and middle-aged adult $Ca_v1.2^{+/-}$ and $Ca_v1.3^{+/-}$ mice compared with age-matched C57 mice, which serve as the background strain control for both heterozygote mice. As illustrated in Figure 9, the $Ca_v1.2^{+/-}$ mice had a substantial reduction in the number of surviving neurons, as well as satellite cells, compared with their age-matched controls, at both 8 and 16 weeks of age. The loss of neuronal cells in the $Ca_v1.2^{+/-}$ mouse appeared slightly greater in the basal versus apical turns (Fig. 9*F*,*J* vs *D*,*H*). The $Ca_v1.3^{+/-}$ mouse also showed a greater loss of SGNs versus the C57 age-matched control (Fig. 10). However, the SGN loss in the $Ca_v1.3^{+/-}$ mouse appeared to be confined to the basal turn only (Fig. 10*B*, rightmost, bottom). The confinement of SGN loss to the basal turn of the $Ca_v1.3^{+/-}$ mouse is in marked contrast to the loss of apical SGNs in the $Ca_v1.2^{+/-}$ mouse at both a slightly younger (Fig. 9*D*) and older (Fig. 9*H*) age. Although the sample of heterozygote mice was small, the substantial reduction of surviving neurons later in development compared with their age-matched controls solidifies the possibility that $Ca_v1.2$, and perhaps $Ca_v1.3$ as well, contribute toward survival of SGNs.

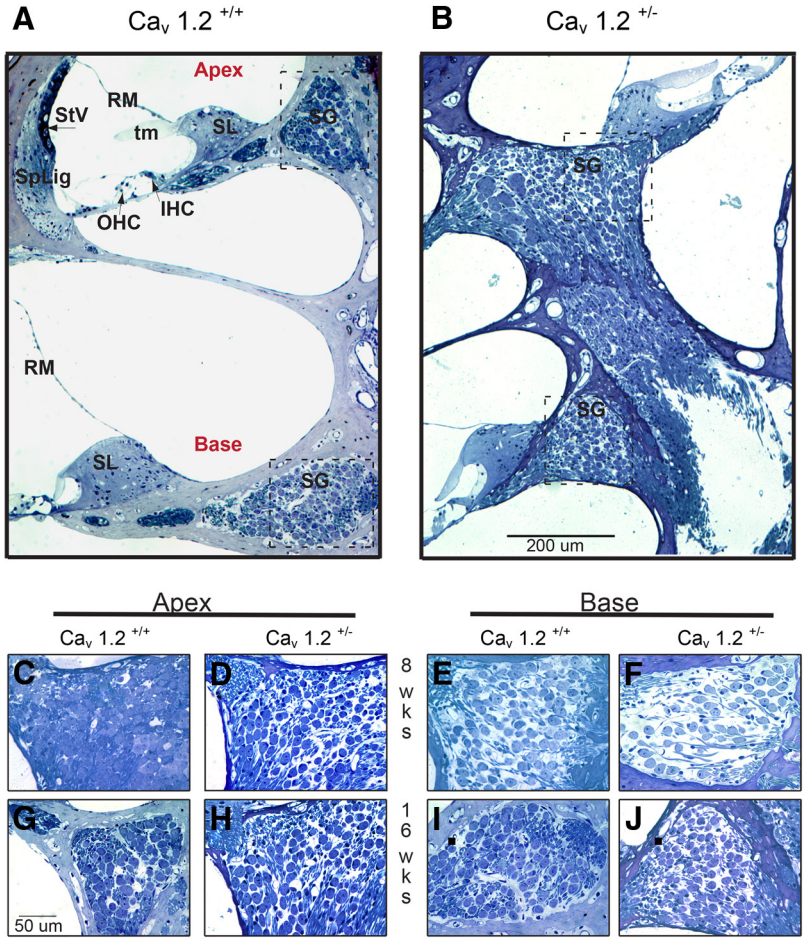


**Figure 9.** Reduced SGN density in $Ca_v1.2$ heterozygote mice. ***A***, ***B***, Modiolar cochlear sections depicting the lower apical (Apex) and basal (Base) turns from a 16-week-old C57BL/6 control (***A***) mouse and a $Ca_v1.2^{+/-}$ (***B***) mouse. Although at this age, a reduction in the number of eighth nerve fibers is expected in the C57 mouse, the density appears even more reduced in the $Ca_v1.2^{+/-}$ mutant. The spiral ganglion regions, outlined in dashes, are shown at higher magnification in ***C–J***. ***C–F***, The spiral ganglion region, shown at higher magnification for the C57BL/6 (***C***, ***E***) and $Ca_v1.3^{+/-}$ (***D***, ***F***) cochlea, is shown for apical (Apex) and basal (Base) turns at 8 weeks of age. In both turns, the packing density of the SGN region appears lower in the $Ca_v1.2^{+/-}$ mouse (***D***, ***F***). ***G–J***, The spiral ganglion region, shown at higher magnification for the C57BL/6 (***G***, ***I***) and $Ca_v1.3^{+/-}$ (***H***, ***J***), is shown for apical (Apex) and basal (Base) turns at 16 weeks of age. The SGN density in the apical turn of the C57BL/6 mouse (***G***) appears higher than that of the age-matched littermate $Ca_v1.2^{+/-}$ mouse (***H***). A higher density in the basal SGN region is also evident between the C57 (***I***) and $Ca_v1.2^{+/-}$ (***J***) mouse. Interestingly, the density of the basal turn SGN region in the 8-week-old C57 and $Ca_v1.2^{+/-}$ mice (***E***, ***F***) appears lower than that of the equivalent SGN area in each strain of mouse at 16 weeks of age (***I***, ***J***). Consistent data were obtained from three different preparations at different ages, using multiple mid-modiolar sections. SG, spiral ganglion; SL, spiral limbus; IHC, inner hair cell; OHC, outer hair cell; tm, tectorial membrane; RM, Reissner's membrane; StV, stria vascularis; SpLig, spiral ligament. Scale bars: ***A***, ***B***, 200 $\mu$m; ***C–J***, 50 $\mu$m.

## Discussion

We have previously demonstrated that SGNs are among the category of neurons that express a variety of $Ca_v$ channels to confer $Ca^{2+}$-dependent functions. The DHP-sensitive current was attributed to $Ca_v1.3$, implicit of its neuronal origin and by immunocytological findings (Xu and Lipscombe, 2001; Lv et al., 2012). In this report, we have shown that the DHP-sensitive currents in SGNs do indeed consist of $Ca_v1.2$ and $Ca_v1.3$ channels. Evaluation of the conductances of the two L-type channels suggest that our previous report was focused on $Ca_v1.2$ channels and not $Ca_v1.3$, as was implied in that study (Lv et al., 2012). We further assert that both channels may have distinct developmental roles such that knockdown of either channel can result in apoptotic cell death. Moreover, maintenance of the integrity of neurites is more likely to be controlled by $Ca_v1.2$ than $Ca_v1.3$. Recordings from isolated SGNs from $Ca_v1.3^{-/-}$ mice showed a significant decrease in the firing frequency of slowly adapting neurons from the basal aspects of the cochlear contour. Features of APs from fast-adapting neurons were unchanged in $Ca_v1.3^{-/-}$ neurons. Careful assessment of the APs from slowly adapting neurons from the $Ca_v1.3^{-/-}$ mice identified prolonged latency and paradoxical increase in AP duration, despite comparable whole-cell $Ca^{2+}$ current densities in the WT and null mutant neurons (Fig. 2). Whole-cell, $Ca^{2+}$ current recordings revealed ~7 mV depolarization shift in the steady-state voltage-dependent activation in $Ca_v1.3^{-/-}$ SGNs compared with the $Ca_v1.3^{+/+}$ neurons. The enduring presence of a DHP-sensitive current in $Ca_v1.3^{-/-}$ SGNs further solidified our prediction that these neurons express two distinct DHP-sensitive $Ca_v$ channels. Although it can be argued that null deletion of the $Ca_v1.3$ gene can result in compensatory expression of an otherwise latent $Ca_v1.2$ gene, direct recordings of single-channel fluctuations from WT SGNs, showing Bay K 8644-sensitive conductances (pS) of ~22 and ~28, substantiated the evidence that two distinct DHP-sensitive channels are present in SGNs. Expression of $Ca_v1.2$ and 1.3 was confirmed and knockdown of the channels

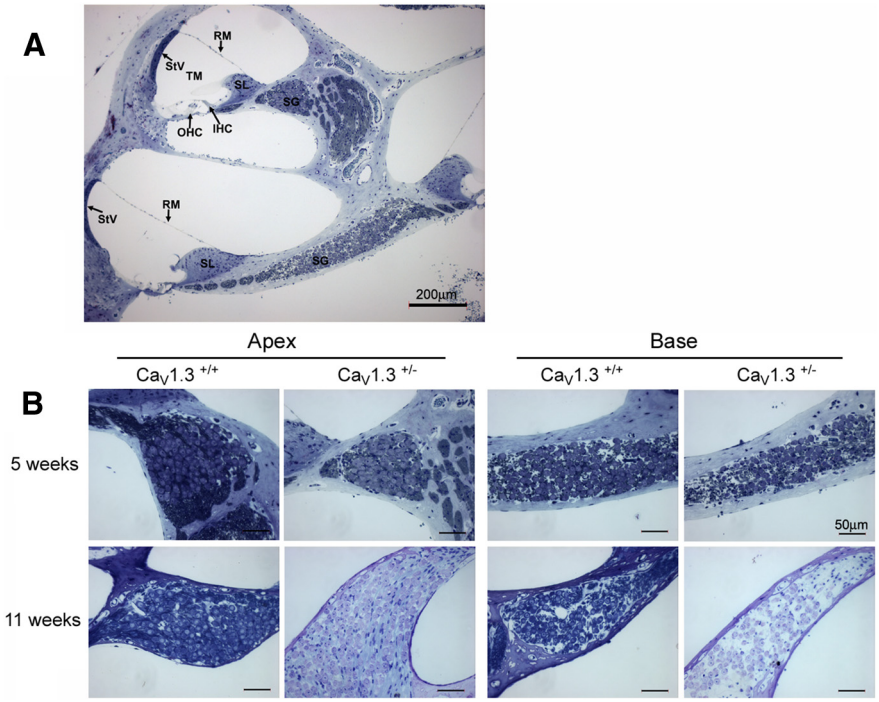


**Figure 10.** Reduced SGN density in *$Ca_v1.3$* heterozygote mice. ***A***, Modiolar cochlear sections depicting the lower apical and basal turns from a 5-week-old C57BL/6 control mouse. At this age, no reduction in the number of eighth nerve fibers is expected in the C57BL/6 mouse. The spiral ganglion regions for this mouse are shown at higher magnifications (***B***, bottom). ***B***, The spiral ganglion region, shown at higher magnifications for the C57BL/6 (left) and *$Ca_v1.3^{+/-}$* (right), is shown for apical (Apex) and basal (Base) turns at 5 weeks of age (top) and at 11 weeks of age (bottom). No difference is evident in the four images from the 5-week-old mice (top). However, a reduction in density in the spiral ganglion area is evident in the base of the *$Ca_v1.3^{+/-}$* mouse at 11 weeks of age (bottom right) when compared with an equivalent region in the C57BL/6 basal SGN region (bottom, second image from right). In contrast, equivalent areas of the SGN region in the apical turn of the *$Ca_v1.3^{+/-}$* mouse and C57BL/6 mouse do not show any differences in the packing density. Consistent data were obtained from three different preparations at different ages, using multiple mid-modiolar sections. SG, spiral ganglion; SL, spiral limbus; IHC, inner hair cell; OHC, outer hair cell; TM, tectorial membrane; RM, Reissner's membrane; StV, stria vascularis. Scale bars: ***A***, 200 $\mu$m ***B***, 50 $\mu$m.

produced apoptotic neuronal death. Finally, we demonstrate that expression of a single copy of *$Ca_v1.2$* and *$Ca_v1.3$* resulted in differential and time-dependent tonotopic degeneration of SGNs, implicating a development and maintenance role for $Ca_v1.2$, and perhaps for the $Ca_v1.3$ channel as well.

### Functional roles of $Ca_v1.2$ channels in SGNs

The findings from this study are in line with the previous concept that SGNs express L-type $Ca^{2+}$ channels (Hisashi et al., 1995) and indirect pharmacological evidence that also implicated L-, N-, and P/Q-type $Ca^{2+}$ channels (Roehm et al., 2008). More recently, direct functional assessment of mature neurons have clearly demonstrated that SGNs harbor L-, N-, P/Q-, R-, and T-type $Ca^{2+}$ channels (Lv et al., 2012). $Ca_v1.2$ channels were identified in SGNs (Waka et al., 2003; Chen et al., 2011), and null deletion of $Ca_v1.2$ in SGNs appears to reduce susceptibility to noise-induced hearing loss (Zuccotti et al., 2013). Moreover, until now, it had not been demonstrated whether $Ca_v1.2$ channels are indeed functional in SGNs. Using a *$Ca_v1.3$*-null deletion mouse model, and direct single-channel recordings from WT neurons, we have demonstrated that SGNs express functional $Ca_v1.2$ channels. The prevalence of $Ca_v1.2$ channels in SGNs is further substantiated by re-evaluation of the conductance of the L-type channels reported previously, such that it is more likely to be $Ca_v1.2$ than $Ca_v1.3$ channels (Lv et al., 2012).

Long-term activation of $Ca^{2+}$ signaling pathways may control gene expression in a distinctive fashion. Gomez-Ospina et al. (2006) have revealed that in addition to $Ca^{2+}$ ions, a fragment of the C termini of $Ca_v1.2$ channel-associated transcription regulator, serves as a transcription factor. Specifically, $Ca_v1.2$ is important for activation of transcription factors that have important roles in promoting neuronal survival and dendritic arborization, such as CREB. Indeed, it has been demonstrated that $Ca^{2+}$ inflow through $Ca_v1.2$ is responsible for activation of $Ca^{2+}$ responsive binding protein, which serves as a *cis*-acting element that encodes brain-derived neurotrophic factor (BDNF) exon IV promoter to regulate the neurotrophin (NT) in an activity-dependent manner (West et al., 2001). BDNF and NT3 are required for cochlear development (Fariñas et al., 1994; Lefebvre et al., 1994; Ernfors et al., 1995), and since their receptors remain robustly expressed after the maturation of hearing, it raises the possibility that both NTs are required to maintain and prevent neuronal degeneration (Miller et al., 1997; Fritzsch et al., 1999; Rubel and Fritzsch, 2002). Thus, for SGNs, the importance of these findings may stem from the prospects that $Ca^{2+}$ inflow through $Ca_v1.2$ may be the underlying mechanism for the maintenance and potential rescue from neuronal degeneration. It remains to be addressed whether direct electrical stimulation of SGNs via an implanted electrode, which increases SGN survival after hair cell loss (Mitchell et al., 1997; Leake et al., 1999), is mediated through activity-dependent activation of $Ca_v1.2$.

### Functional roles of $Ca_v1.3$ channels in SGNs

Our data remain consistent with the previous notion that $Ca_v1.3$ channels are among one of the multiple $Ca^{2+}$ channels in SGNs (Lv et al., 2012), and it is also in agreement with studies that demonstrated $Ca_v1.3$ channels are low voltage-activated (Xu and Lipscombe, 2001). After null deletion of *$Ca_v1.3$*, the voltage-dependent activation properties of the whole-cell $Ca^{2+}$ currents were shifted rightward by ~7 mV. Since the recordings in Figure 2*E* were performed at a holding potential of −50 mV, we anticipate that other low voltage-activated $Ca^{2+}$ channel (T-type, $Ca_v3.x$) currents in SGNs were suppressed by increased inactivation (Lv et al., 2012). Significant prolongation of the AP latency in the *$Ca_v1.3^{-/-}$* basal SGNs supports the prediction that the current likely contributes toward the upstroke phase of APs. Although the $Ca^{2+}$ current densities in the *$Ca_v1.3^{+/+}$* and *$Ca_v1.3^{-/-}$* SGNs remained unchanged, predictably because of compensatory changes in the mutant mice (Zhang et al., 2002), AP duration was unexpectedly prolonged in basal neurons. These findings raise the possibility that activation of the $Ca_v1.3$ channel may be functionally coupled with a $Ca^{2+}$-dependent outward current. Indeed, a similar conclusion was made in a study of cardiac myocytes in which the AP prolongation in *$Ca_v1.3^{-/-}$*

mice was attributed to abnormal function of the small conductance $Ca^{2+}$-activated $K^+$ (SK) channels (Lu et al., 2007). The unique specificity of functional coupling between $Ca^{2+}$ channels and $Ca^{2+}$-activated $K^+$ channels has also been demonstrated in hippocampal neurons (Marrion and Tavalin, 1998). For SGNs, additional experiments are required to identify the potential outward current associated with $Ca_v1.3$ and the ensuing mechanisms, and their functional relevance. Moreover, the nuances of the significance of expression of two distinct DHP-sensitive $Ca^{2+}$ channels in SGNs remain to be disentangled fully.

## References


Bean BP (1984) Nitrendipine block of cardiac calcium channels: high-affinity binding to the inactivated state. Proc Natl Acad Sci U S A 81: 6388–6392. CrossRef Medline

Bell DC, Butcher AJ, Berrow NS, Page KM, Brust PF, Nesterova A, Stauderman KA, Seabrook GR, Nürnberg B, Dolphin AC (2001) Biophysical properties, pharmacology, and modulation of human, neuronal L-type (alpha(1D), Ca(V)1.3) voltage-dependent calcium currents. J Neurophysiol 85:816–827. Medline

Borst JG, Sakmann B (1998) Facilitation of presynaptic calcium currents in the rat brainstem. J Physiol 513:149–155. CrossRef Medline

Cao XJ, Oertel D (2010) Auditory nerve fibers excite targets through synapses that vary in convergence, strength, and short-term plasticity. J Neurophysiol 104:2308–2320. CrossRef Medline

Chaudhuri D, Alseikhan BA, Chang SY, Soong TW, Yue DT (2005) Developmental activation of calmodulin-dependent facilitation of cerebellar P-type Ca2+ current. J Neurosci 25:8282–8294. CrossRef Medline

Chen WC, Xue HZ, Hsu YL, Liu Q, Patel S, Davis RL (2011) Complex distribution patterns of voltage-gated calcium channel alpha-subunits in the spiral ganglion. Hear Res 278:52–68. CrossRef Medline

Dou H, Vazquez AE, Namkung Y, Chu H, Cardell EL, Nie L, Parson S, Shin HS, Yamoah EN (2004) Null mutation of alpha1D Ca2+ channel gene results in deafness but no vestibular defect in mice. J Assoc Res Otolaryngol 5:215–226. Medline

Dunlap K, Luebke JI, Turner TJ (1995) Exocytotic Ca2+ channels in mammalian central neurons. Trends Neurosci 18:89–98. CrossRef Medline

Ernfors P, Van De Water T, Loring J, Jaenisch R (1995) Complementary roles of BDNF and NT-3 in vestibular and auditory development. Neuron 14:1153–1164. CrossRef Medline

Fariñas I, Jones KR, Backus C, Wang XY, Reichardt LF (1994) Severe sensory and sympathetic deficits in mice lacking neurotrophin-3. Nature 369:658–661. CrossRef Medline

Fritzsch B, Pirvola U, Ylikoski J (1999) Making and breaking the innervation of the ear: neurotrophic support during ear development and its clinical implications. Cell Tissue Res 295:369–382. CrossRef Medline

Gomez-Ospina N, Tsuruta F, Barreto-Chang O, Hu L, Dolmetsch R (2006) The C terminus of the L-type voltage-gated calcium channel Ca(V)1.2 encodes a transcription factor. Cell 127:591–606. CrossRef Medline

Hamill OP, Marty A, Neher E, Sakmann B, Sigworth FJ (1981) Improved patch-clamp techniques for high-resolution current recording from cells and cell-free membrane patches. Pflugers Arch 391:85–100. CrossRef Medline

Hegarty JL, Kay AR, Green SH (1997) Trophic support of cultured spiral ganglion neurons by depolarization exceeds and is additive with that by neurotrophins or cAMP and requires elevation of [Ca2+]i within a set range. J Neurosci 17:1959–1970. Medline

Hisashi K, Nakagawa T, Yasuda T, Kimitsuki T, Komune S, Komiyama S (1995) Voltage-dependent Ca2+ channels in the spiral ganglion cells of guinea pig cochlea. Hear Res 91:196–201. CrossRef Medline

Howard MA, Rubel EW (2010) Dynamic spike thresholds during synaptic integration preserve and enhance temporal response properties in the avian cochlear nucleus. J Neurosci 30:12063–12074. CrossRef Medline

Imredy JP, Yue DT (1992) Submicroscopic Ca2+ diffusion mediates inhibitory coupling between individual Ca2+ channels. Neuron 9:197–207. CrossRef Medline

Imredy JP, Yue DT (1994) Mechanism of Ca(2+)-sensitive inactivation of L-type Ca2+ channels. Neuron 12:1301–1318. CrossRef Medline

Leake PA, Hradek GT, Snyder RL (1999) Chronic electrical stimulation by a cochlear implant promotes survival of spiral ganglion neurons after neonatal deafness. J Comp Neurol 412:543–562. CrossRef Medline

Lefebvre PP, Malgrange B, Staecker H, Moghadass M, Van de Water TR, Moonen G (1994) Neurotrophins affect survival and neuritogenesis by adult injured auditory neurons in vitro. Neuroreport 5:865–868. CrossRef Medline

Levic S, Nie L, Tuteja D, Harvey M, Sokolowski BH, Yamoah EN (2007) Development and regeneration of hair cells share common functional features. Proc Natl Acad Sci U S A 104:19108–19113. CrossRef Medline

Lu L, Zhang Q, Timofeyev V, Zhang Z, Young JN, Shin HS, Knowlton AA, Chiamvimonvat N (2007) Molecular coupling of a Ca2+-activated K+ channel to L-type Ca2+ channels via alpha-actinin2. Circ Res 100:112–120. CrossRef Medline

Lv P, Wei D, Yamoah EN (2010) Kv7-type channel currents in spiral ganglion neurons: involvement in sensorineural hearing loss. J Biol Chem 285:34699–34707. CrossRef Medline

Lv P, Sihn CR, Wang W, Shen H, Kim HJ, Rocha-Sanchez SM, Yamoah EN (2012) Posthearing Ca(2+) currents and their roles in shaping the different modes of firing of spiral ganglion neurons. J Neurosci 32:16314–16330. CrossRef Medline

Marrion NV, Tavalin SJ (1998) Selective activation of Ca2+-activated K+ channels by colocalized Ca2+ channels in hippocampal neurons. Nature 395:900–905. CrossRef Medline

Michna M, Knirsch M, Hoda JC, Muenkner S, Langer P, Platzer J, Striessnig J, Engel J (2003) Cav1.3 (alpha1D) Ca2+ currents in neonatal outer hair cells of mice. J Physiol 553:747–758. CrossRef Medline

Miller JM, Chi DH, O'Keeffe LJ, Kruszka P, Raphael Y, Altschuler RA (1997) Neurotrophins can enhance spiral ganglion cell survival after inner hair cell loss. Int J Dev Neurosci 15:631–643. CrossRef Medline

Mitchell A, Miller JM, Finger PA, Heller JW, Raphael Y, Altschuler RA (1997) Effects of chronic high-rate electrical stimulation on the cochlea and eighth nerve in the deafened guinea pig. Hear Res 105:30–43. CrossRef Medline

Mochida S, Few AP, Scheuer T, Catterall WA (2008) Regulation of presynaptic Ca(V)2.1 channels by Ca2+ sensor proteins mediates short-term synaptic plasticity. Neuron 57:210–216. CrossRef Medline

Namkung Y, Skrypnyk N, Jeong MJ, Lee T, Lee MS, Kim HL, Chin H, Suh PG, Kim SS, Shin HS (2001) Requirement for the L-type Ca(2+) channel alpha(1D) subunit in postnatal pancreatic beta cell generation. J Clin Invest 108:1015–1022. CrossRef Medline

Olivera BM, Miljanich GP, Ramachandran J, Adams ME (1994) Calcium channel diversity and neurotransmitter release: the omega-conotoxins and omega-agatoxins. Annu Rev Biochem 63:823–867. CrossRef Medline

Platzer J, Engel J, Schrott-Fischer A, Stephan K, Bova S, Chen H, Zheng H, Striessnig J (2000) Congenital deafness and sinoatrial node dysfunction in mice lacking class D L-type Ca2+ channels. Cell 102:89–97. CrossRef Medline

Poncer JC, McKinney RA, Gähwiler BH, Thompson SM (1997) Either N- or P-type calcium channels mediate GABA release at distinct hippocampal inhibitory synapses. Neuron 18:463–472. CrossRef Medline

Rodriguez-Contreras A, Yamoah EN (2001) Direct measurement of single-channel Ca(2+) currents in bullfrog hair cells reveals two distinct channel subtypes. J Physiol 534:669–689. CrossRef Medline

Rodríguez-Contreras A, Yamoah EN (2003) Effects of permeant ion concentrations on the gating of L-type Ca2+ channels in hair cells. Biophys J 84:3457–3469. CrossRef Medline

Rodriguez-Contreras A, Nonner W, Yamoah EN (2002) Ca2+ transport properties and determinants of anomalous mole fraction effects of single voltage-gated Ca2+ channels in hair cells from bullfrog saccule. J Physiol 538:729–745. CrossRef Medline

Rodriguez-Contreras A, Lv P, Zhu J, Kim HJ, Yamoah EN (2008) Effects of strontium on the permeation and gating phenotype of calcium channels in hair cells. J Neurophysiol 100:2115–2124. CrossRef Medline

Roehm PC, Xu N, Woodson EA, Green SH, Hansen MR (2008) Membrane depolarization inhibits spiral ganglion neurite growth via activation of multiple types of voltage sensitive calcium channels and calpain. Mol Cell Neurosci 37:376–387. CrossRef Medline

Rubel EW, Fritzsch B (2002) Auditory system development: primary auditory neurons and their targets. Annu Rev Neurosci 25:51–101. CrossRef Medline

Rutherford MA, Chapochnikov NM, Moser T (2012) Spike encoding of neurotransmitter release timing by spiral ganglion neurons of the cochlea. J Neurosci 32:4773–4789. CrossRef Medline

Schnee ME, Ricci AJ (2003) Biophysical and pharmacological characteriza-

tion of voltage-gated calcium currents in turtle auditory hair cells. J Physiol 549:697–717. CrossRef Medline

Tadross MR, Dick IE, Yue DT (2008) Mechanism of local and global Ca2+ sensing by calmodulin in complex with a Ca2+ channel. Cell 133:1228–1240. CrossRef Medline

Trussell LO (1997) Cellular mechanisms for preservation of timing in central auditory pathways. Curr Opin Neurobiol 7:487–492. CrossRef Medline

Waka N, Knipper M, Engel J (2003) Localization of the calcium channel subunits Cav1.2 (alpha1C) and Cav2.3 (alpha1E) in the mouse organ of Corti. Histol Histopathol 18:1115–1123. Medline

Wei D, Jin Z, Järlebark L, Scarfone E, Ulfendahl M (2007) Survival, synaptogenesis, and regeneration of adult mouse spiral ganglion neurons in vitro. Dev Neurobiol 67:108–122. CrossRef Medline

Wei D, Levic S, Nie L, Gao WQ, Petit C, Jones EG, Yamoah EN (2008) Cells of adult brain germinal zone have properties akin to hair cells and can be used to replace inner ear sensory cells after damage. Proc Natl Acad Sci U S A 105:21000–21005. CrossRef Medline

West AE, Chen WG, Dalva MB, Dolmetsch RE, Kornhauser JM, Shaywitz AJ, Takasu MA, Tao X, Greenberg ME (2001) Calcium regulation of neuronal gene expression. Proc Natl Acad Sci U S A 98:11024–11031. CrossRef Medline

Wheeler DB, Randall A, Tsien RW (1994) Roles of N-type and Q-type Ca2+ channels in supporting hippocampal synaptic transmission. Science 264:107–111. CrossRef Medline

Xu J, Wu LG (2005) The decrease in the presynaptic calcium current is a major cause of short-term depression at a calyx-type synapse. Neuron 46:633–645. CrossRef Medline

Xu W, Lipscombe D (2001) Neuronal Ca(V)1.3alpha(1) L-type channels activate at relatively hyperpolarized membrane potentials and are incompletely inhibited by dihydropyridines. J Neurosci 21:5944–5951. Medline

Zampini V, Johnson SL, Franz C, Lawrence ND, Münkner S, Engel J, Knipper M, Magistretti J, Masetto S, Marcotti W (2010) Elementary properties of CaV1.3 Ca(2+) channels expressed in mouse cochlear inner hair cells. J Physiol 588:187–199. CrossRef Medline

Zhang Z, Xu Y, Song H, Rodriguez J, Tuteja D, Namkung Y, Shin HS, Chiamvimonvat N (2002) Functional Roles of $Ca_{(v)}1.3$ (alpha(1D)) calcium channel in sinoatrial nodes: insight gained using gene-targeted null mutant mice. Circ Res 90:981–987. CrossRef Medline

Zuccotti A, Lee SC, Campanelli D, Singer W, Satheesh SV, Patriarchi T, Geisler HS, Köpschall I, Rohbock K, Nothwang HG, Hu J, Hell JW, Schimmang T, Rüttiger L, Knipper M (2013) L-type *$Ca_V1.2$* deletion in the cochlea but not in the brainstem reduces noise vulnerability: implication for $Ca_V1.2$-mediated control of cochlear BDNF expression. Front Mol Neurosci 6:20. CrossRef Medline